International Journal of Microwave and Wireless Technologies

cambridge.org/mrf

Self-octuplexing substrate-integrated waveguide semi-elliptical-shaped slot antenna for multifunctional communication systems

Swapnil Shekhar[1], Kundan Kumar[3], Shruti Priya[2], Nitesh Kashyap[3] and Surinder Singh[4]

[1]Department of Electrical Engineering, Indian Institute of Technology Delhi, New Delhi, India; [2]Department of Electronics Engineering, Indian Institute of Technology (ISM), Dhanbad, India; [3]Department of Electronics and Communication Engineering, Dr. B. R. Ambedkar National Institute Technology, Jalandhar, India and [4]Department of Electronics and Communication Engineering, Sant Longowal Institute of Engineering and Technology, Sangrur, India

Research Paper

Cite this article: Shekhar S, Kumar K, Priya S, Kashyap N, Singh S (2026) Self-octuplexing substrate-integrated waveguide semi-elliptical-shaped slot antenna for multifunctional communication systems. *International Journal of Microwave and Wireless Technologies* **18**(1), 82–98. https://doi.org/10.1017/S175907872610302X

Received: 7 February 2025
Revised: 14 February 2026
Accepted: 22 February 2026

Keywords:
high isolation; low cross polarization; octagonal SIW cavity; self-octuplexing; unperturbed ground plane

Corresponding author: Kundan Kumar; Email: kundansingh.singh5@gmail.com

Abstract

This paper presents a novel self-octuplexing substrate-integrated waveguide (SIW) cavity-backed slot antenna for eight-band wireless communication services. This antenna employs eight semi-elliptical-shaped slots on an octagonal SIW cavity with different lengths to radiate at eight different frequencies. The eight radiating frequencies are 2.7, 3, 3.3, 3.6, 3.9, 4.2, 4.5, and 4.72 GHz, with impedance matching is less than −10 dB. Each radiator is backed by an eighth-mode SIW cavity and excited by a 50 Ω microstrip line. A designed prototype of the antenna is fabricated and tested. It has more than 34 dB measured isolation among any two ports. The maximum measured antenna gains are 4.4, 4.19, 4.11, 4.03, 4.19, 4.28, 5.2, and 5.44 dBi at the respective operating frequencies. It has a measured cross-polarization level of below −24.2 dB in the boresight direction and a front-to-back ratio of more than 10.4 dB in all the bands. All the slots can be tuned independently to radiate at the desired frequency band. This antenna can easily be integrated with other planar circuits due to an unperturbed ground plane.

Introduction

Recent trends in advanced wireless communication technology have increased the demand for versatile multiband antennas that support multiple frequency bands for ubiquitous connectivity [1]. The modern RF front-end communication systems function simultaneously at different communication standards with increased data transfer capacity, enabling expansion into many new services and application areas, such as the Internet of Things, mission-critical communications, healthcare, and military [2, 3]. Traditionally, multiple antennas were integrated into a system to support applications operating at different frequencies. Hence, single-port multiband antennas [3–5] were introduced to achieve the functionality of multiple antennas with increased portability and reduced physical size, complexity, and cost. However, transmission or reception of the data is restricted to a particular frequency band at a time due to the inherent antenna structure resulting from the shared antenna aperture and single-port design. Shared aperture multiband antenna design topology requires external filters or multiplexer circuits for frequency band selection, resulting in additional hardware, increased coupling, and unwanted noise among components connected with the port [6, 7]. Therefore, researchers have proposed self-multiplexing antennas (SMAs) using substrate-integrated waveguides (SIWs) technology to address the issues with multiband antennas [8–23]. SMA has individual ports for each band, improving the isolation between ports without external circuits and enabling simultaneous operation in multiple frequency bands. Several SMAs are implemented using the SIW cavity-backed slot antenna approach, as it offers compactness, high gain, unidirectional radiation pattern, and high front-to-back ratio (FTBR) while maintaining the planar form. SMAs up to six ports, such as self-diplexing antennas [8, 9], self-triplexing antennas [10, 11], self-quadruplexing antennas [12, 13], self-quintuplexing antennas [14–16], and self-hexaplexing antennas [17–20], have been proposed recently. A limited number of self-octuplexing antennas are available in the open literature [21–23]. Papers [21] and [23] have poor isolation, while [21–23] have a low co-to-cross polarization difference. Also, the coaxial feed from the bottom ground plane in [23] restricts the integration in planar systems.

This paper proposes a novel SIW cavity-backed self-octuplexing slot antenna with high isolation and high co-to-cross polarization difference for octa-band wireless communication applications. The designed antenna consists of eight different semi-elliptical-shaped slots in an octagonal SIW cavity. The eight radiating frequencies are 2.7, 3, 3.3, 3.6, 3.9, 4.2, 4.5,

© The Author(s), 2026. Published by Cambridge University Press in association with The European Microwave Association.

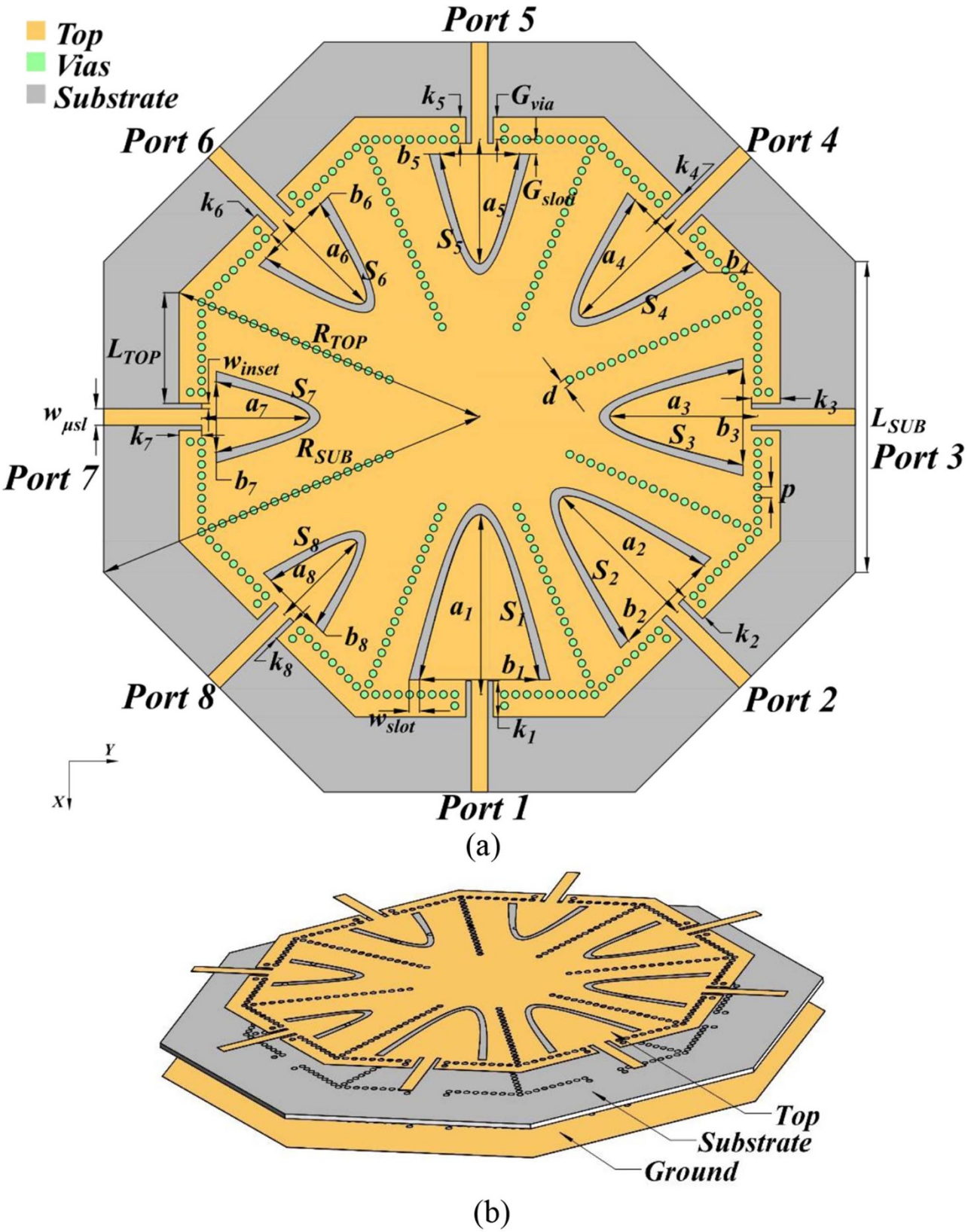


Figure 1. (a) Schematic diagram and (b) exploded view of the proposed self-octuplexing antenna ($S_1 = 47.77$, $S_2 = 42.74$, $S_3 = 38.42$, $S_4 = 34.74$, $S_5 = 31.71$, $S_6 = 29.29$, $S_7 = 27.09$, $S_8 = 25.37$, $a_1 = 23.94$, $a_2 = 21.64$, $a_3 = 19.64$, $a_4 = 17.94$, $a_5 = 16.54$, $a_6 = 15.34$, $a_7 = 14.34$, $a_8 = 13.64$, $b_1 = 15.96$, $b_2 = 14.2$, $b_3 = 12.8$, $b_4 = 11.6$, $b_5 = 10.6$, $b_6 = 10.2$, $b_7 = 9.4$, $b_8 = 8.4$, $k_1 = 4.8$, $k_2 = 3.7$, $k_3 = 3.8$, $k_4 = 3.8$, $k_5 = 3.5$, $k_6 = 3.2$, $k_7 = 3$, $k_8 = 3.2$, $p = 1.5$, $d = 1$, $w_{slot} = 1.4$, $G_{via} = 3$, $G_{sloti} = 1.94$, $w_{inset} = 0.7$, $w_{\mu sl} = 2.2$, $L_{TOP} = 14.74$, $L_{SUB} = 41.37$, $R_{TOP} = 43.23$, and $R_{SUB} = 54.05$; unit: mm).

https://doi.org/10.1017/S175907872610302X Published online by Cambridge University Press

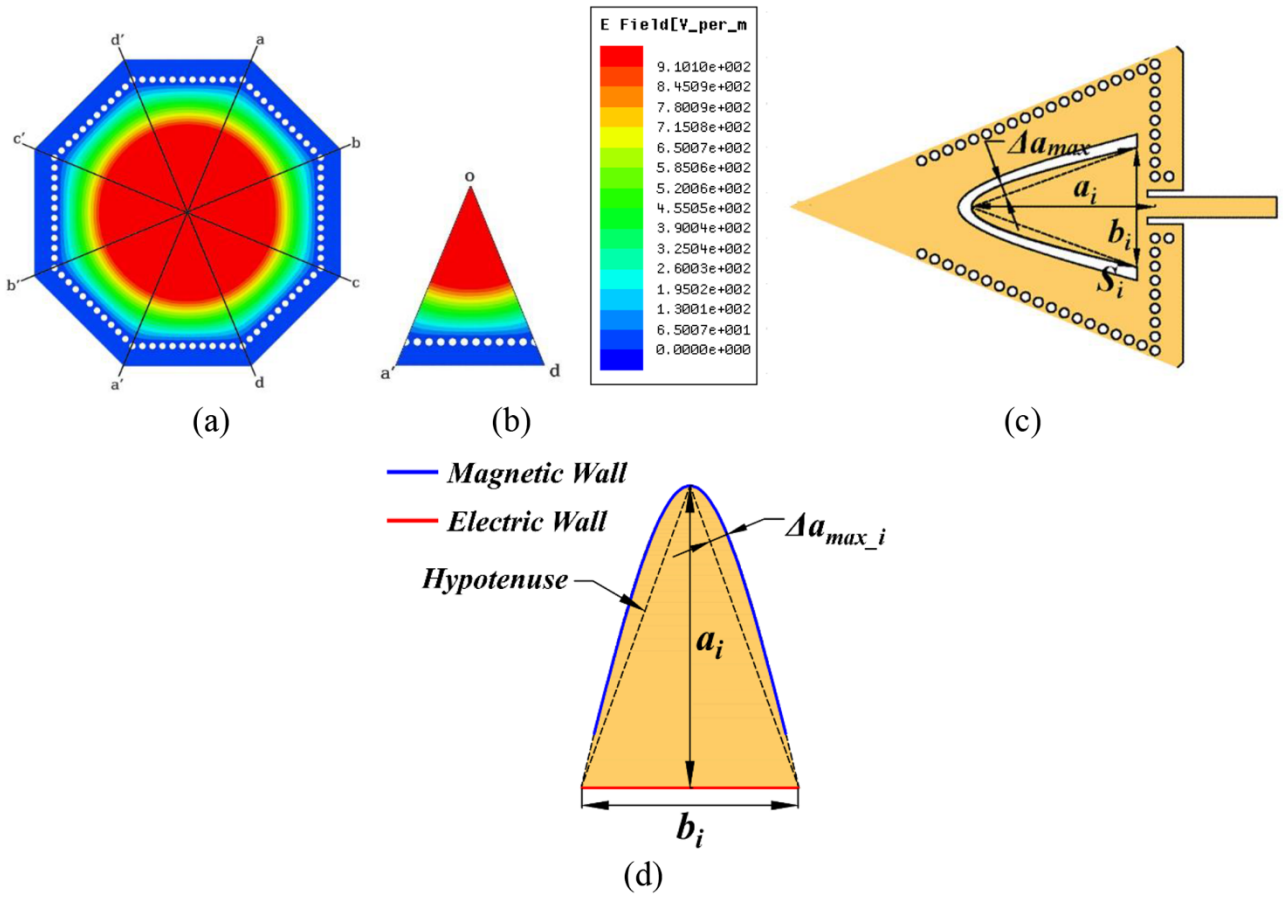


Figure 2. Electric field distribution in SIW cavity in (a) fundamental mode, (b) one-eighth mode, (c) geometry of a single radiating element backed by OEMSIW cavity, and (d) one-eighth-mode radiator represented with electric wall and magnetic wall.

and 4.72 GHz. Each radiator is backed by a one-eighth-mode SIW (OEMSIW). All eight frequency bands can be tuned independently. The antenna has at least a measured isolation of 34 dB among the any two ports, a measured co-to-cross polarization level of below −24.2 dB and measured gains of more than 4 dBi in all bands.

Antenna configuration

Figure 1(a) and 1(b) shows the top view of the proposed self-octuplexing antenna design with optimized dimensions and the exploded view of the modelled antenna. The antenna is designed on a 0.787 mm thick single-layer Roger RT/Duroid 5880 substrate with a dielectric constant (ε_r) of 2.2 and a loss tangent (tan δ) of 0.0009. Eight semi-elliptical-shaped slots of different lengths are etched on the top of the octagonal SIW cavity to radiate at eight different frequencies. The radiating cavities of the antenna are fed by a microstrip line. The antenna is designed and analyzed using a 3D electromagnetic (EM) computer-aided simulation software tool, Ansys's high-frequency structure simulator.

Antenna design and analysis

The fundamental mode cavity of the proposed antenna can be divided into eight equal parts along four diagonal lines, aa′, *bb*′, *cc*′, and *dd*′, as shown in Figure 2(a). Figure 2(b) shows the extracted OEMSIW cavity. The radius of the octagonal top patch (R_{TOP}) is selected to ensure that the OEMSIW cavity can accommodate the largest semi-elliptical radiator slot designed to operate at the lowest resonant frequency while providing adequate margin for frequency tuning and fabrication constraints. An OEMSIW cavity backs each radiating slot of the antenna. Radiating slots of three different shapes, semi-elliptical, triangular, and semicircular, were designed and simulated. Eight slots with dimensions to radiate at the desired operating frequency were placed in the OEMSIW cavity for each shape. The semi-elliptical slots required the least open arc edge length (S_i) to achieve radiation at the target frequency among the three shapes. For instance, as considered for port number 1, the semi-elliptical slot is able to radiate at 2.7 GHz frequency with a smaller open arc edge length, reduced by 8.3% and 22.4% as compared to the triangular and semicircular slots' open arc edge length radiating at the same frequency. Similarly, for the case when the open arc edge length of the three different-shaped slots was equal, the operating frequency of semi-elliptical slot for port 1 was 8.46% and 19.73% lower as compared to the operating frequency of the triangular and semicircular slots with the same open arc edge length. An improvement in isolation among ports is also observed for semi-elliptical slot radiators in both the simulation scenarios mentioned. The maximum difference between co-to-cross polarization occurs at a slot width (w_{slot}) of 1.4 mm. Any deviation from this optimal width reduces the co-to-cross polarization difference [12]. The width of the microstrip line ($w_{\mu sl}$), the width of the inset (w_{inset}), and the length of the inset (k_i) are considered such that each slot cavity of the antenna is fed by the respective matched

https://doi.org/10.1017/S175907872610302X Published online by Cambridge University Press

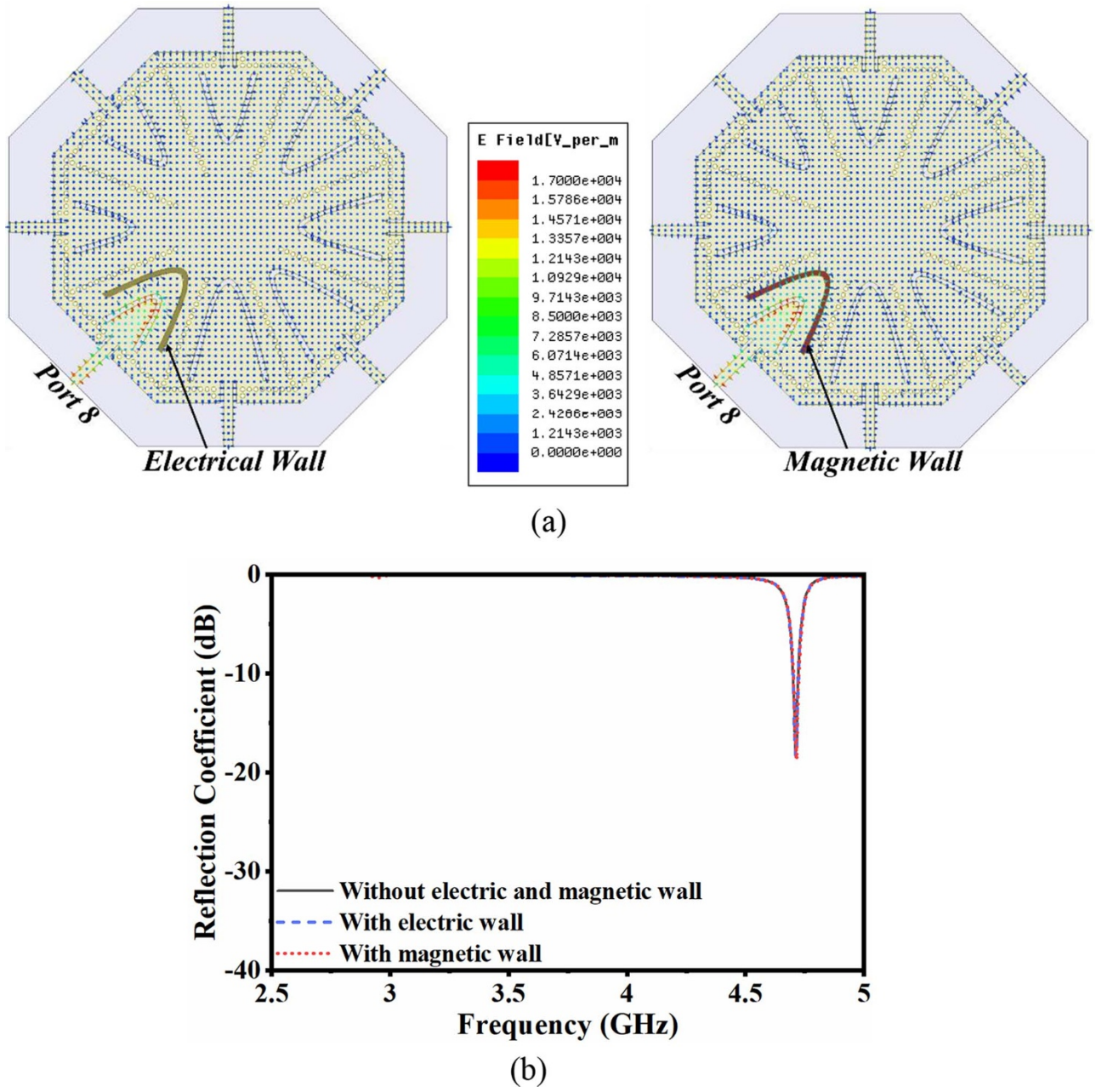


Figure 3. (a) Vector electric field distribution at 4.72 GHz for port 8 with a perfect electric and a perfect magnetic wall placed inside the OEMSIW cavity. (b) Reflection coefficient comparison when port 8 is excited.

microstrip line to maintain reflection coefficients less than −15 dB. A representative diagram of an individual radiating element is shown in Figure 2(c). The resonator of the presented antenna works in one-eighth mode of the fundamental TE_{110} mode. The resonant frequency of each radiator can be calculated using Equation (1) [24]

$$f_{mn0} = \frac{c}{2\pi\sqrt{\varepsilon_{eff}}}\sqrt{\left(\frac{m\pi}{2(a_i + 2\Delta a_{max_i})}\right)^2 + \left(\frac{n\pi}{4b_i}\right)} \quad (1)$$

where m and n are mode indices, c is the speed of an EM wave in a vacuum, ε_{eff} is the effective dielectric constant of the substrate ($\varepsilon_{eff} = \frac{(\varepsilon_r+1)}{2}$), and ε_r is the relative permittivity of the substrate. Here, a_i signifies the length from the vertex of the inner edge of the semi-elliptical slot, and b_i signifies the base width of the respective ith port, as shown in Figure 2(c) and 2(d). Δa_{max_i} is the maximum perpendicular distance between the arc of the semi-elliptical slot facing the port and the hypotenuse of the triangle, which has a height of a_i and a base width of $b_i/2$, as shown in Figure 2(d). The value of a_i and b_i should be at least $\lambda_g/2$ and $\lambda_g/4$, respectively, where λ_g ($= \lambda_0/\sqrt{\varepsilon_r}$) is the guided wavelength at the operating frequency. Specifically in OEMSIW, the length is halved along the a_i dimension, and the width is quartered along the b_i dimension compared to a full-mode waveguide, resulting in half-wavelength and quarter-wavelength resonances along the respective dimensions. Due to the loading effect, the resonant frequency of the radiator

https://doi.org/10.1017/S175907872610302X Published online by Cambridge University Press

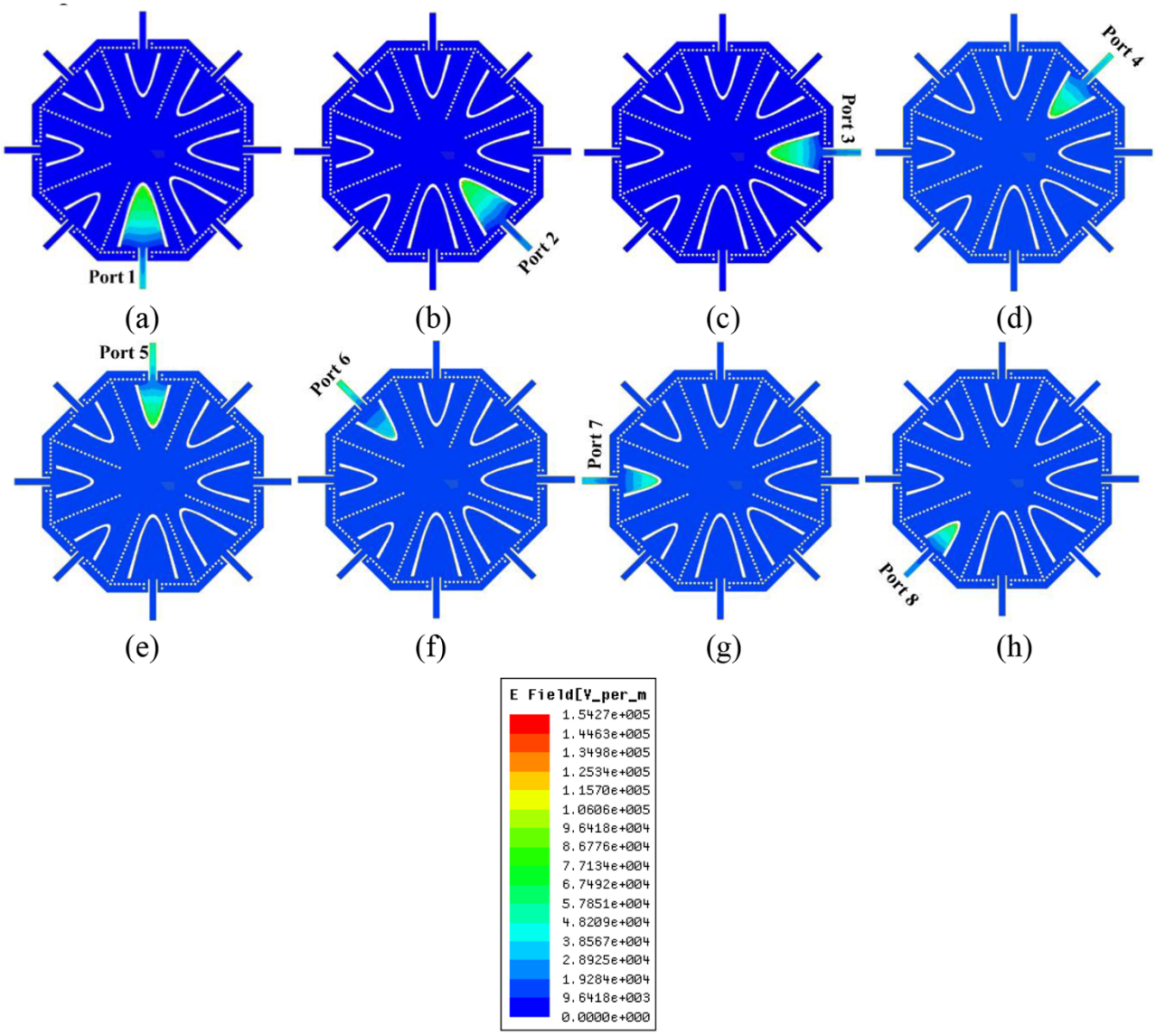


Figure 4. Electric-field distributions when (a) port 1, (b) port 2, (c) port 3, (d) port 4, (e) port 5, (f) port 6, (g) port 7, and (h) port 8 are excited individually.

is slightly deviated from the frequency obtained from (1). Hence, this equation is only used as an initial design guideline.

E-field distribution

The power supplied to an individual port can be coupled with the other radiators, which leads to poor isolation. Therefore, vias are introduced on the diagonals of the octagon according to the design rule (2) to reduce the power coupling among the radiators and increase the isolation between ports [25]

$$p < 2.5\,d \tag{2}$$

where p is the pitch, the longitudinal spacing between centers of two adjacent vias, and d is the diameter of the via. The minimum simulated isolation between any two ports, without vias on the diagonals, was −19.8 dB. When vias were placed along the full length of the four diagonals, minimum simulated isolation improved significantly to −30 dB. Therefore, the number of vias along the diagonals was optimized to maintain high isolation between the ports without significantly increasing fabrication complexity. The vias act as an electrical wall and confine the electric field in the intended cavity. A semi-elliptical-shaped perfect electric and perfect magnetic conductor wall is placed adjacent to the etched radiator for port number 8 without altering the dimensions of the cavity. The cavity dimensions are kept intact. For analyzing the surface EM energy distribution, a perfect electric conductor wall (PECW) and a perfect magnetic conductor wall (PMCW) are introduced just above the slot of port 8. Figure 3(a) illustrates the vector electric field distribution for the cases with PECW and PMCW. It is observed that the z-directed electric field corresponding to the TE_{10} mode of the eighth-mode cavity excites the odd mode of the slotline. Nearly 100% radiation efficiency is achieved with a radiating slot width of 1.4 mm. However, a further increase in the slot width degrades the cross-polarization performance [12]. Figure 3(b) presents the reflection coefficient responses for three cases: without any wall, with PECW, and with PMCW. The reflection characteristics show close agreement in all three cases, indicating negligible EM energy leakage to other ports

https://doi.org/10.1017/S175907872610302X Published online by Cambridge University Press

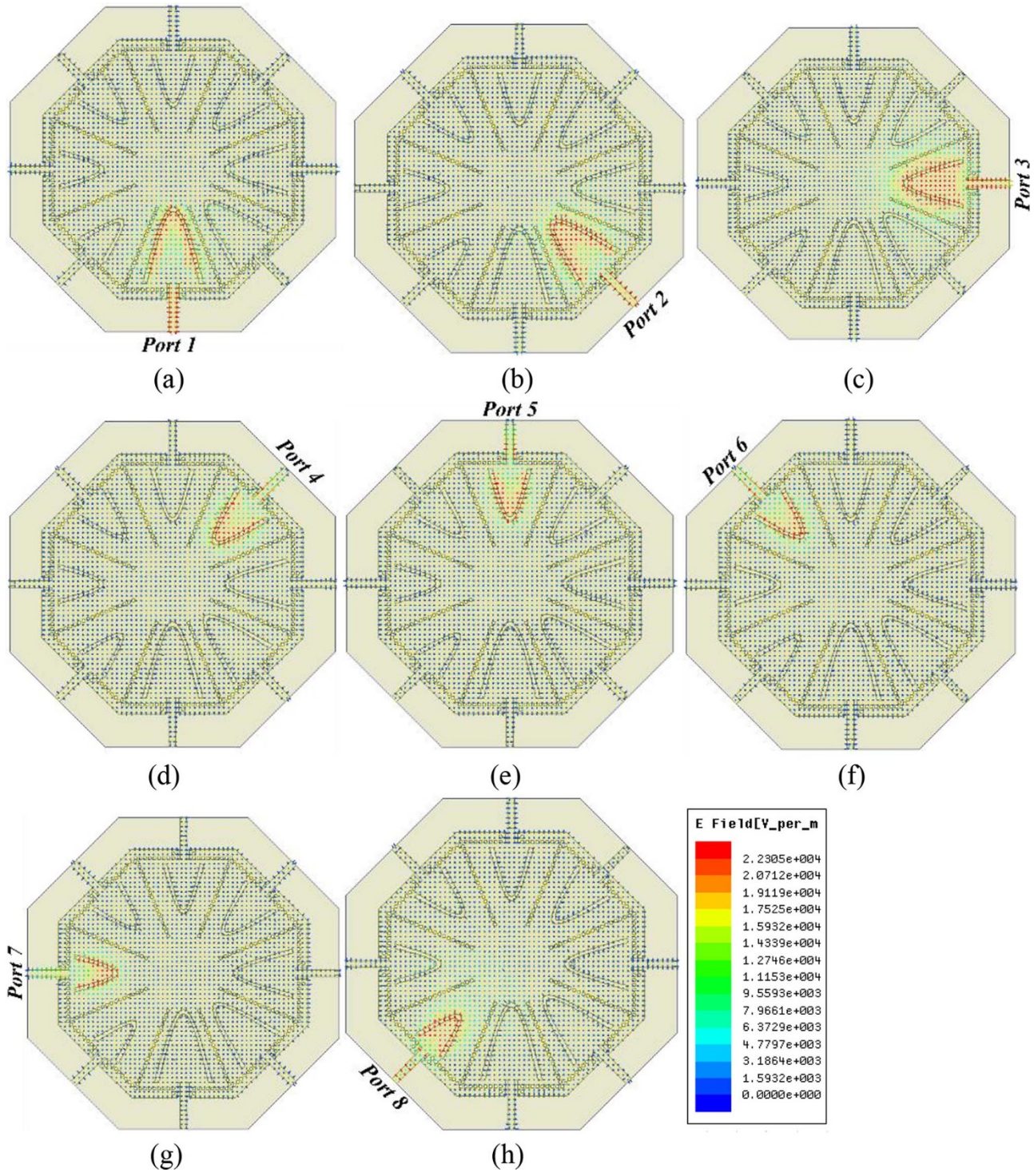


Figure 5. Vector electric-field distributions when (a) port 1, (b) port 2, (c) port 3, (d) port 4, (e) port 5, (f) port 6, (g) port 7, and (h) port 8 are excited individually.

through the cavity surface. This confirms that almost all the input energy is radiated through the slots. Consequently, very high isolation (greater than 30 dB) is maintained among the radiation cavities. The electric field distribution when a single port is excited individually is shown in Figure 4(a)–4(h). Each divided cavity supports the perturbed one-eighth of TE_{110} mode, as evident by the electric field distribution. The signal propagates from an excited port and radiates upon encountering a discontinuity in the form of the corresponding designed semi-elliptical slot. The resonant frequency of the radiated field depends on the dimension of the open edge of the slot. This radiation is primarily due to the fringing electric fields at the edges of the slot, as shown by the vector

https://doi.org/10.1017/S175907872610302X Published online by Cambridge University Press

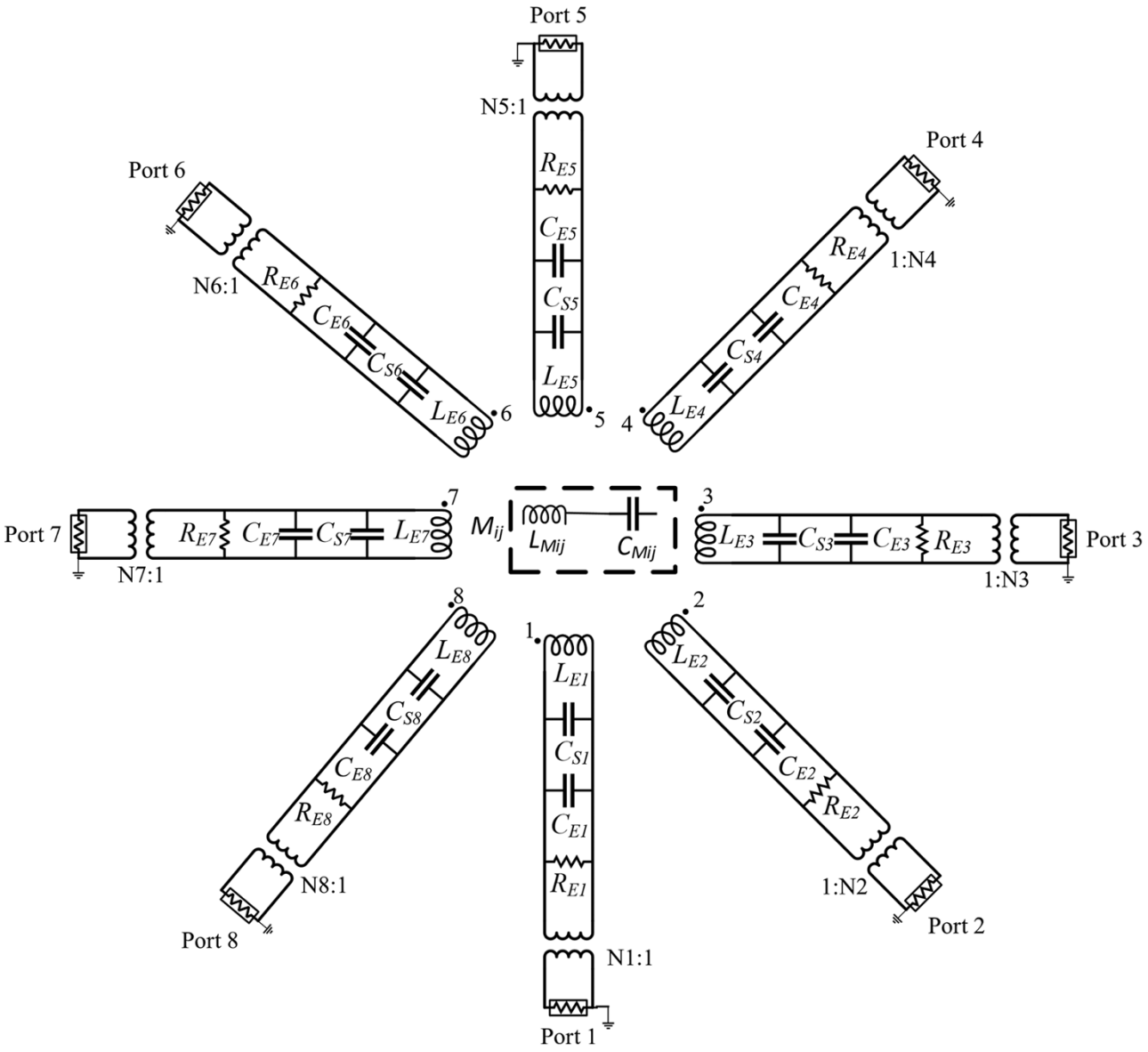


Figure 6. Equivalent circuit of the proposed self-octuplexing antenna.

electric field distribution of the proposed antenna for each port in Figure 5(a)–5(h).

Equivalent circuit model

The equivalent circuit model serves as a benchmark for simulating the antenna's complex EM behavior in terms of lumped electrical circuit components like resistors, inductors, and capacitors. A circuit model simplifies the analysis and enables smoother integration in complex systems where antennas are part of larger electronic systems. Therefore, a schematic diagram of the equivalent circuit model of the proposed self-octuplexing antenna is presented in Figure 6. The circuit model is designed, simulated, and validated using Keysight Advanced Design System software. The values of the lumped elements and the turn ratio are iteratively optimized till there is a significant agreement in the *S* parameter values of the circuit and EM model of the proposed antenna. The optimized value of the lumped circuit components is given in Table 1. Here, R_{Ei} is resistance, C_{Ei} is capacitance, and L_{Ei} is inductance associated with the individual cavity of the ports, and i signifies the port number varying from 1 to 8. A parallel resistor (R), inductor (L), and capacitor (C) (RLC) circuit can represent each one-eighth cavity resonator. The eight radiating elements, etched in the form of semi-elliptical ring-shaped slots etched on the octagonal resonator, act as shunt capacitors and are represented by C_{Si}. A series LC circuit is used as an equivalent circuit to model mutual coupling (M_{ij}) between any two ports, numbered i and j, where $i \neq j$. C_{Mij} represents mutual capacitance, and L_{Mij} represents mutual inductance between the ports. The transformers Ni (i = 1–8) represent the impedance matching between the ports and the RLC circuit networks. The resonant frequency and the input impedance of the resonators are determined by (3) and (4) [26].

$$f_{0i} = \frac{1}{2\pi\sqrt{L_{Ei}C_{Si}}} \tag{3}$$

https://doi.org/10.1017/S175907872610302X Published online by Cambridge University Press

Table 1. Value of components of the circuit model

Comp.	Value	Comp.	Value	Comp.	Value	Comp.	Value
R_{E1}	436.25	L_{E1}	0.25000	C_{E1}	0.300097	C_{S1}	14.24029
R_{E2}	423.50	L_{E2}	0.19587	C_{E2}	0.600940	C_{S2}	14.34230
R_{E3}	398.25	L_{E3}	0.15090	C_{E3}	2.100790	C_{S3}	13.76530
R_{E4}	373.75	L_{E4}	0.19887	C_{E4}	0.643920	C_{S4}	9.569520
R_{E5}	312.25	L_{E5}	0.10993	C_{E5}	0.100990	C_{S5}	15.37523
R_{E6}	359.50	L_{E6}	0.11092	C_{E6}	0.304970	C_{S6}	12.97935
R_{E7}	364.25	L_{E7}	0.12292	C_{E7}	0.333970	C_{S7}	10.14649
R_{E8}	400.75	L_{E8}	0.15291	C_{E8}	1.100890	C_{S8}	6.612670
$L_{M1,2}$	69.00054	$C_{M1,2}$	36.80008	$L_{M3,5}$	32.40019	$C_{M3,5}$	31.20022
$L_{M1,3}$	39.00074	$C_{M1,3}$	30.00	$L_{M3,6}$	30.00100	$C_{M3,6}$	28.80028
$L_{M1,4}$	30.15	$C_{M1,4}$	29.70	$L_{M3,7}$	31.20022	$C_{M3,7}$	30.00000
$L_{M1,5}$	30.00	$C_{M1,5}$	30.00	$L_{M3,8}$	30.00200	$C_{M3,8}$	30.00200
$L_{M1,6}$	30.30	$C_{M1,6}$	29.90	$L_{M4,5}$	48.00068	$C_{M4,5}$	26.40034
$L_{M1,7}$	30.25	$C_{M1,7}$	30.13	$L_{M4,6}$	30.00400	$C_{M4,6}$	29.99700
$L_{M1,8}$	30.20	$C_{M1,8}$	30.10	$L_{M4,7}$	30.00400	$C_{M4,7}$	29.99600
$L_{M2,3}$	72.00052	$C_{M2,3}$	29.99	$L_{M4,8}$	28.80328	$C_{M4,8}$	29.99600
$L_{M2,4}$	29.70	$C_{M2,4}$	30.00	$L_{M5,6}$	28.80028	$C_{M5,6}$	31.20022
$L_{M2,5}$	30.00	$C_{M2,5}$	30.02	$L_{M5,7}$	33.60016	$C_{M5,7}$	30.00025
$L_{M2,6}$	30.05	$C_{M2,6}$	30.20	$L_{M5,8}$	30.00025	$C_{M5,8}$	30.00025
$L_{M2,7}$	30.00300	$C_{M2,7}$	30.00025	$L_{M6,7}$	40.00000	$C_{M6,7}$	28.80028
$L_{M2,8}$	31.20022	$C_{M2,8}$	28.80028	$L_{M6,8}$	28.80028	$C_{M6,8}$	28.80028
$L_{M3,4}$	57.00062	$C_{M3,4}$	15.00900	$L_{M7,8}$	70.50053	$C_{M7,8}$	27.60031
N1	0.4	N3	0.4	N5	0.4	N7	0.4
N2	0.4	N4	0.4	N6	0.4	N8	0.4

Notes: Comp. stands for Component; Units: Resistance = Ω, inductance = nH, and capacitance = pF.

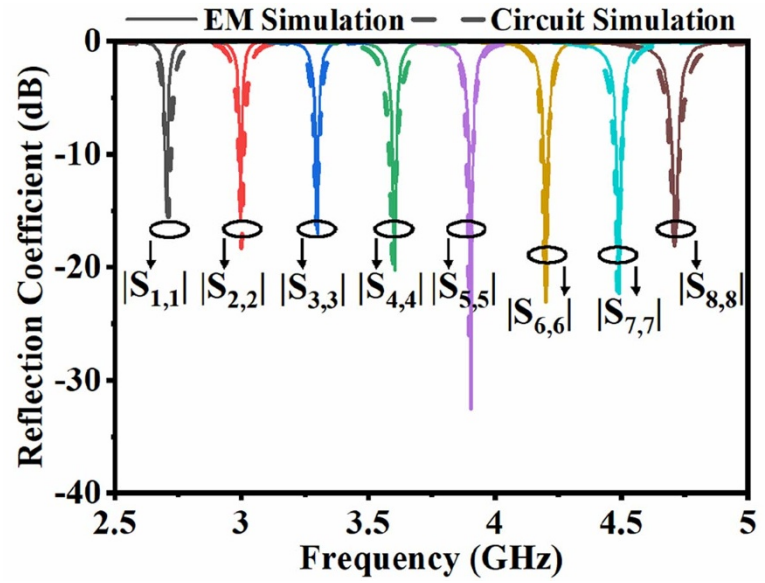


Figure 7. Reflection coefficient for EM and circuit simulation of the proposed antenna.

https://doi.org/10.1017/S175907872610302X Published online by Cambridge University Press

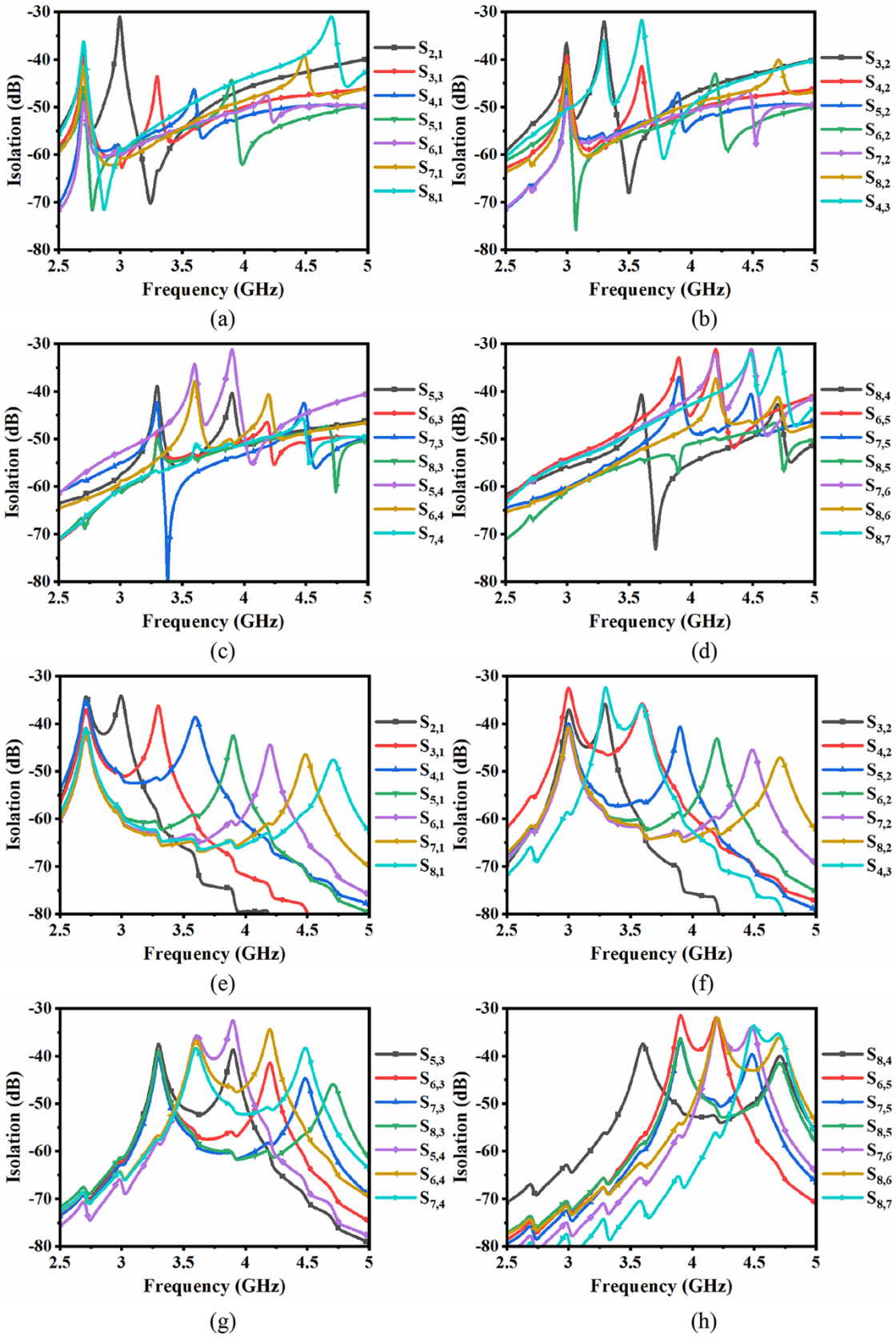


Figure 8. Isolation for (a)–(d) EM simulation and (e)–(h) circuit simulation of the proposed antenna.

https://doi.org/10.1017/S175907872610302X Published online by Cambridge University Press

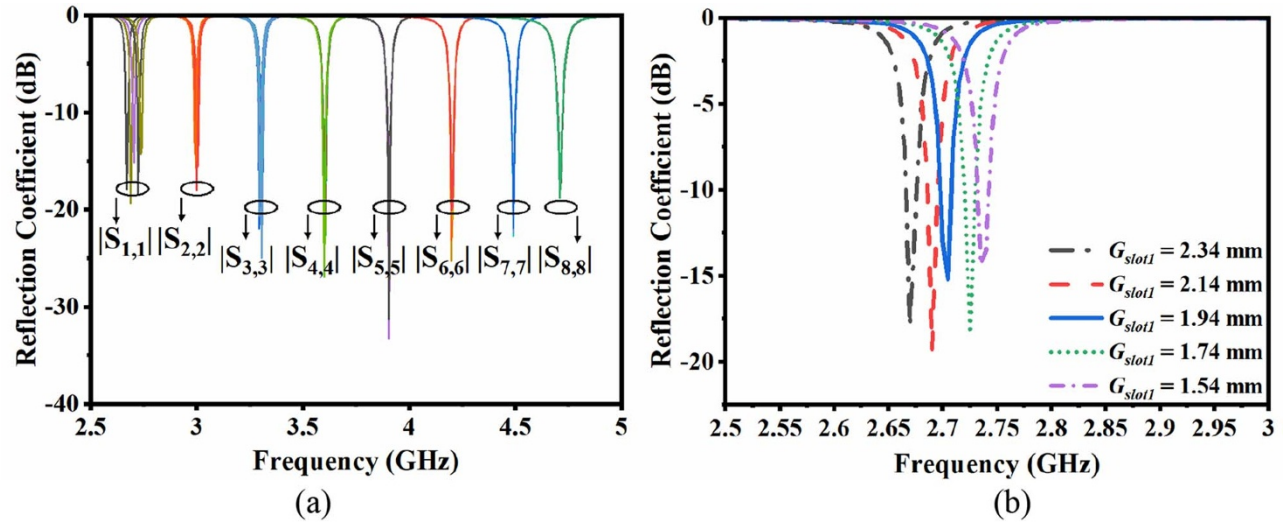


Figure 9. Variation in reflection coefficient with G_{slot1} keeping other dimensions constant (a) port 1, (b) magnified view of frequency variation.

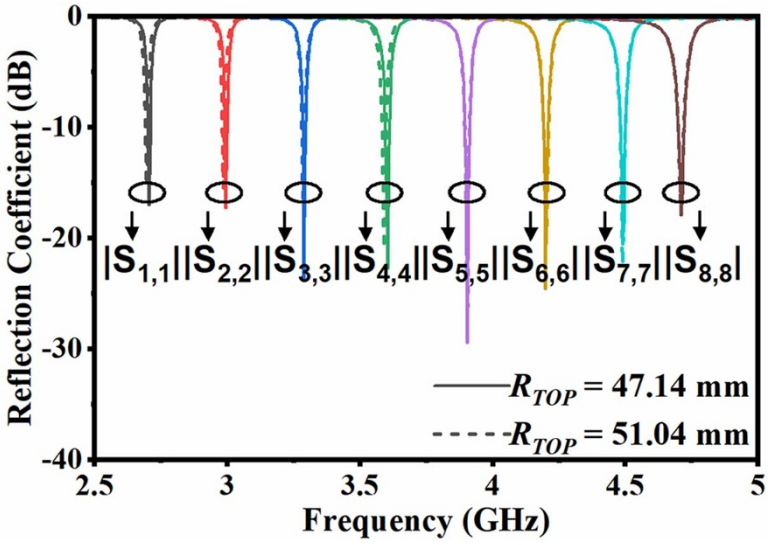


Figure 10. Reflection coefficient for different values of R_{TOP}.

The input impedance is given by

$$Z_{in} = \frac{j\omega_{0i}L_{Ei}}{1 - \omega_{0i}^2 L_{Ei}C_{Si}} \quad (4)$$

The resonant frequency is inversely proportional to the shunt capacitance C_{Si} as given in Equation (3), and the slot dimension is directly proportional to the shunt capacitance. Therefore, when the slot dimension is increased, the associated capacitance increases, decreasing the resonant frequency. The antenna's resonant frequency can be varied by changing the slot dimension. Hence, the miniaturization of the antenna can be achieved by reducing the slot dimensions. The comparison between the reflection coefficient obtained from EM simulation and circuit simulation is given in Figure 7. There is a notable agreement between the reflection coefficient values obtained from EM simulations and those derived from circuit simulations. The isolation values between any two ports exceed 30 dB in both simulations, as shown in Figure 8, which depicts the comparison between circuit simulation's and EM simulation's isolation values.

Tuning of operating frequencies

The proposed antenna design allows easy tuning of each resonant frequency independently using a single variable G_{sloti}, where G_{sloti} is the distance of the respective *i*th slot from the vias at the periphery. Figure 1 shows a representative G_{sloti} for a single slot. A parallel resonant circuit represents an unperturbed one-eighth-mode cavity. A shunt capacitance in the equivalent parallel RLC circuit model represents the radiating slot. Therefore, when the slot is moved radially inwards, the capacitance increases. As the resonant frequency is inversely proportional to capacitance, hence the resonant frequency decreases. Figure 9 shows the variation in reflection coefficient at the resonant frequency due to changes in the radial position of the slot for $G_{slot1} = 1.54$, 1.74, 1.94, 2.14, and 2.34 mm, with the highest resonant frequency obtained at $G_{slot1} = 1.54$ mm and the lowest resonant frequency obtained at $G_{slot1} = 2.34$ mm. There is no significant effect on other antenna performance characteristics as frequency tuning is performed without altering the initial cavity dimensions. The proposed antenna can be operated at any desired frequency between 2.47 and 4.96 GHz by varying

https://doi.org/10.1017/S175907872610302X Published online by Cambridge University Press

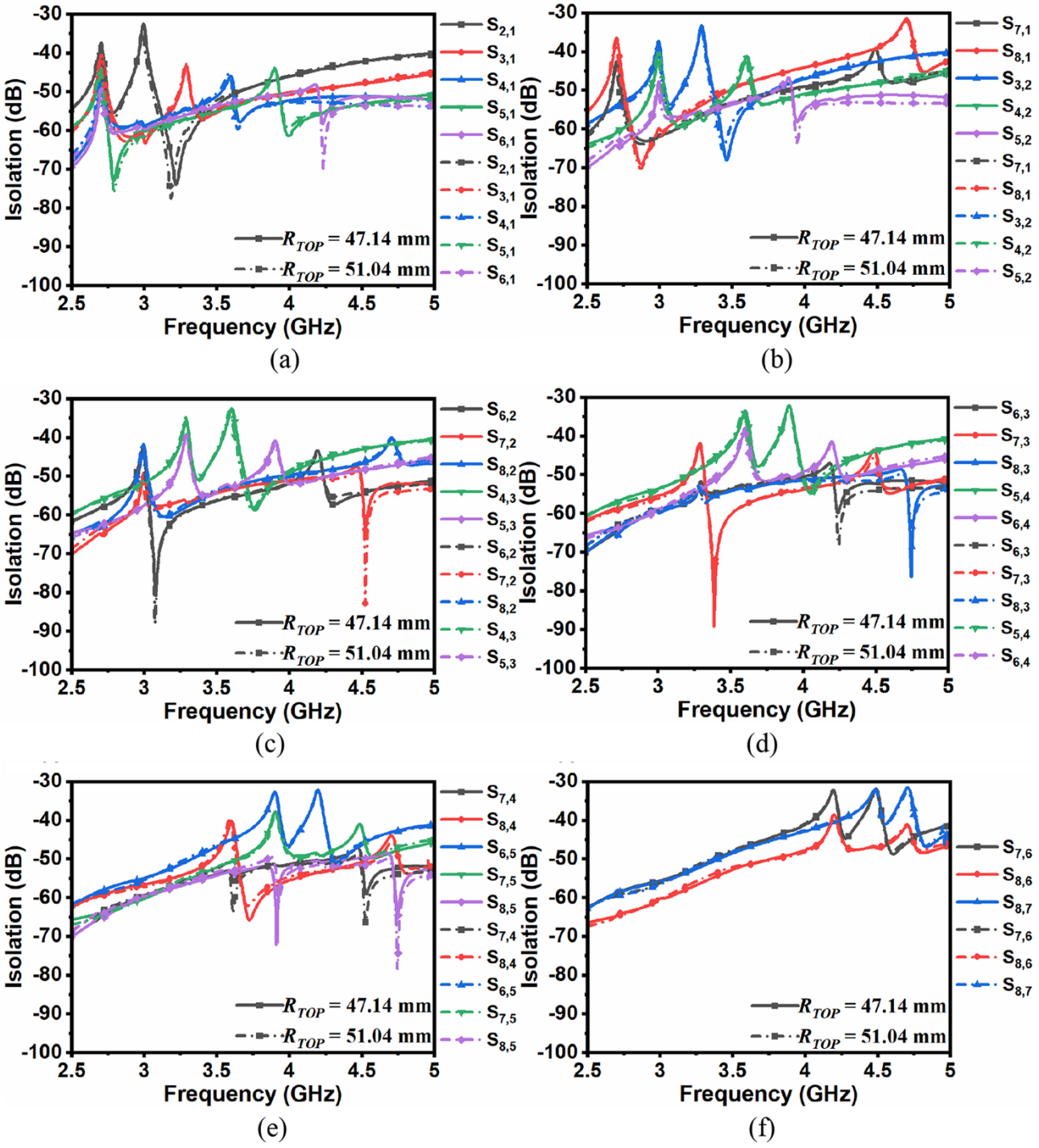


Figure 11. Isolation for different values of R_{TOP}.

the distance of the respective *i*th slot from the vias at the periphery (G_{sloti}). In all the cases, simulated isolation is maintained better than 30 dB.

In addition to slot positioning, the effect of cavity radius, R_{TOP}, on the antenna performance is examined. When cavity radius R_{TOP} is increased while keeping the slots at the same absolute position as in the original design, a decrease in the resonant frequency and poor impedance matching are observed. This behavior is consistent with the explanation discussed above. In this case, increasing the cavity dimension effectively moves the slots radially inward with respect to the new cavity boundary, which increases the dimension a_i from the outer wall of cavity, thus lowering the resonant frequency observed as Equation (1).

In contrast, when R_{TOP} is increased while maintaining the relative distance of each slot from the respective port, that is, preserving the values of G_{sloti} as in the original design, the resonant frequency of the ports remains unchanged since the a_i remains constant, as shown in Figure 10. However, an

https://doi.org/10.1017/S175907872610302X Published online by Cambridge University Press

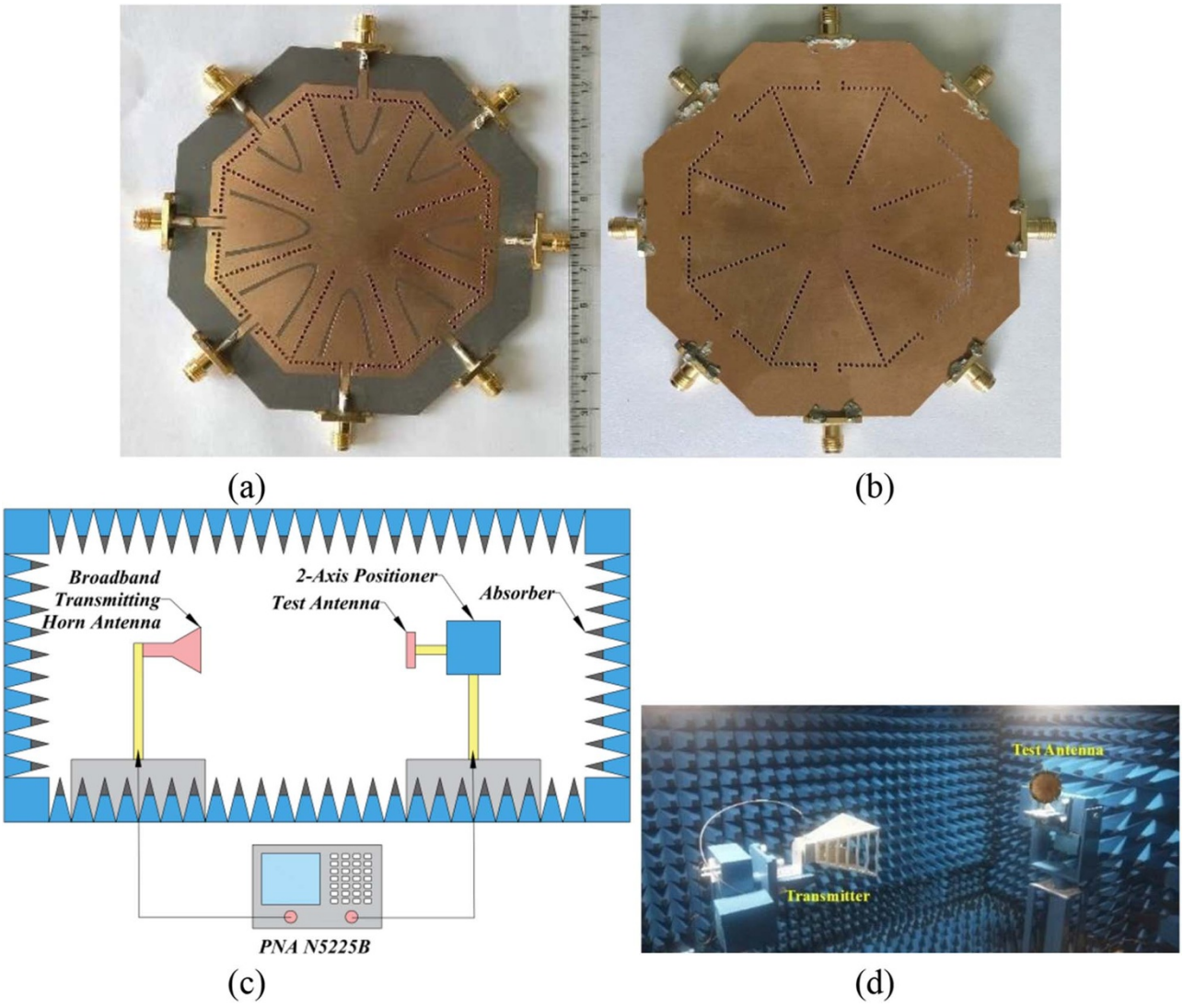


Figure 12. Fabricated antenna structure (a) top view, (b) ground plane view, (c) diagram of measurement setup, and (d) measurement setup in anechoic chamber.

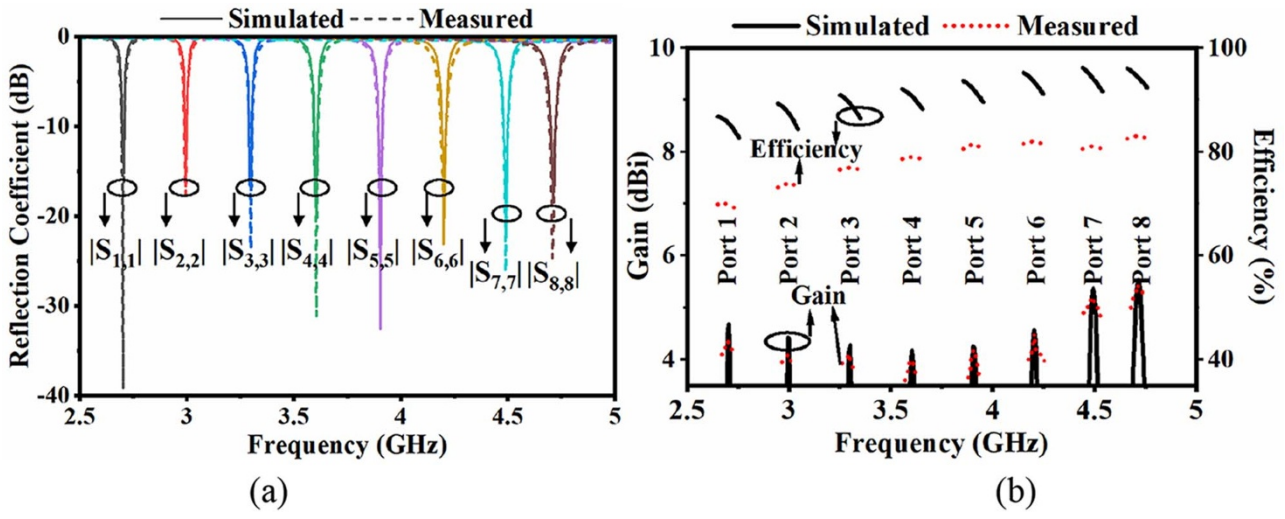


Figure 13. Simulated and measured (a) reflection coefficient and (b) gain and efficiency.

https://doi.org/10.1017/S175907872610302X Published online by Cambridge University Press

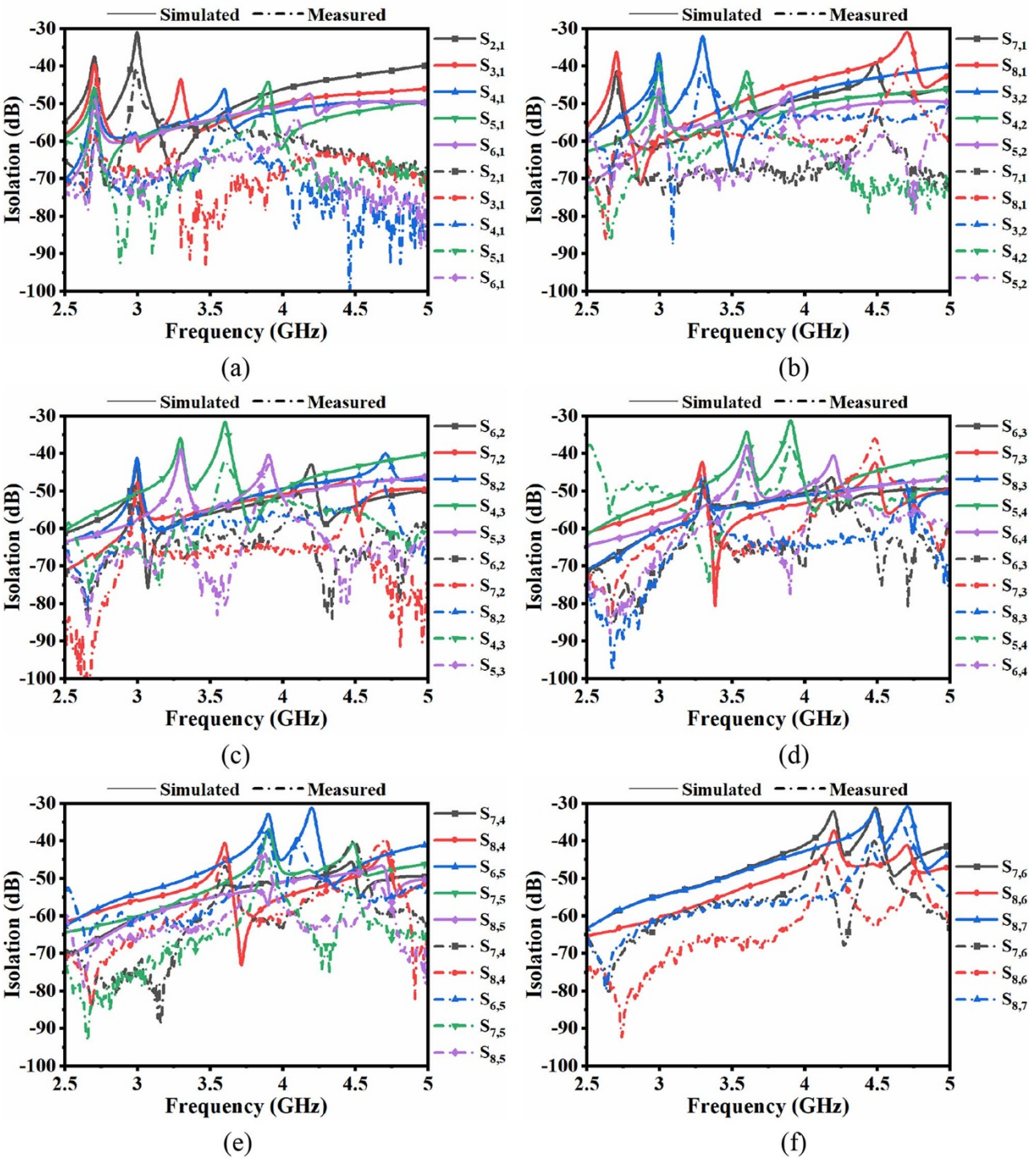


Figure 14. Simulated and measured isolation for the proposed antenna.

improvement of 0.46 dB in minimum isolation is observed due to the increased physical separation between the radiating slots, which occurs with an increase in R_{TOP}. Figure 11(a)–11(f) shows isolation values when R_{TOP} is 47.14 and 51.06 mm. Therefore, the value of R_{TOP} kept optimum to maintain isolation among the elements is better than 30 dB in a smaller antenna size.

The following design steps are suggested based on the above study:

1) Select an octagonal cavity with a dimension of its circumradius $\approx 0.58\,\lambda_g$, where $\lambda_g = \lambda_0/\sqrt{\varepsilon_r}$ at the lowest mid-band frequency.
2) Place the slots with length $\lambda_g/2$, at $\lambda_g/4$ from the respective port, where λ_g corresponds to their respective guided wavelengths.
3) Optimize for $|S_{11}| < -15$ dB for each port by varying the length of the respective inset.
4) Adjust the slot length or slot position to get the desired resonant frequency.

https://doi.org/10.1017/S175907872610302X Published online by Cambridge University Press

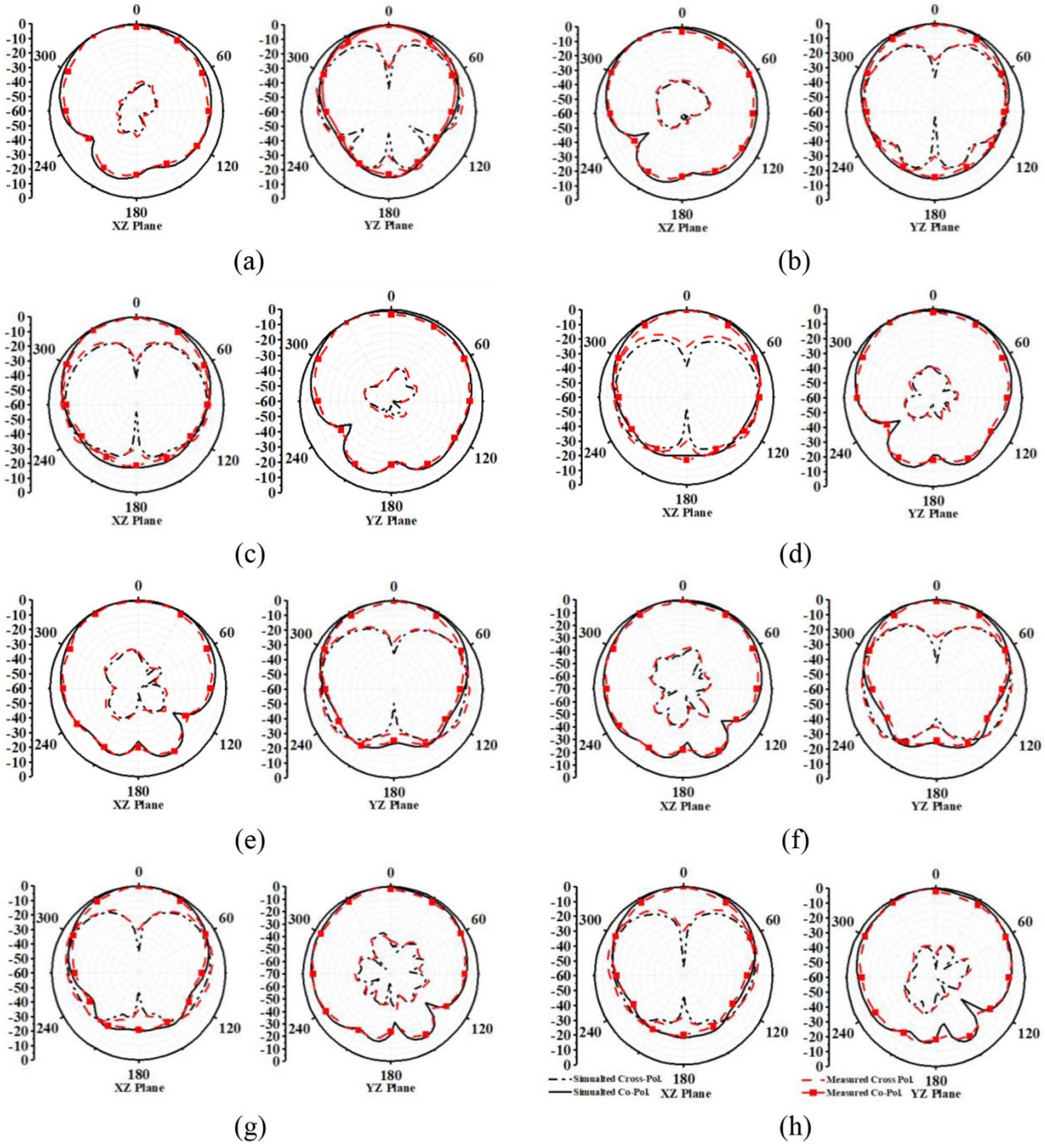


Figure 15. Simulated and measured radiation pattern at (a) 2.7 GHz, (b) 3.0 GHz, (c) 3.3 GHz, (d) 3.6 GHz, (e) 3.9 GHz, (f) 4.2 GHz, (g) 4.5 GHz, and (h) 4.72 GHz.

5) Repeat steps (3) and (4) for each slot till the intended results are obtained.

Result and discussion

The self-octuplexing SIW cavity-backed slot antenna is fabricated on Rogers RT/Duroid 5880 substrate to validate the design. Figure 12(a) shows the top view, and Figure 12(b) shows the ground plane view of the fabricated antenna. The diagram of the measurement setup inside the anechoic chamber is given in Figure 12(c). A broadband horn antenna is used as a transmitting antenna, while the fabricated antenna is placed in a receiving configuration at the receiver side. While measuring the parameters of the fabricated antenna, the excitation is applied sequentially to one port at a time while the remaining unused ports are terminated with 50 Ω matched loads. The excitation signal and the measurement procedure are carried out using a Keysight PNA Network Analyzer N5225B. Figure 12(d) shows the actual measurement setup. There is a significant agreement between the proposed antenna's simulated and measured reflection coefficients, as shown in Figure 13(a). The measured gains and antenna efficiencies

https://doi.org/10.1017/S175907872610302X Published online by Cambridge University Press

Table 2. Measured antenna parameters

Port excited	Resonant frequency (GHz)	Minimum isolation (dB)	Gain (dBi)	Cross polarization (dB)	FTBR (dB)
1	2.7	39.7	4.40	30.09	17.24
2	3.0	40.0	4.19	25.77	13.99
3	3.3	36.0	4.11	30.40	10.56
4	3.6	37.7	4.03	25.49	10.40
5	3.9	37.3	4.19	28.97	10.52
6	4.2	37.3	4.28	24.20	13.98
7	4.5	34.5	5.20	30.84	23.37
8	4.72	34.5	5.44	30.98	27.10

Table 3. Comparison of the proposed self-octuplexing antenna with previous SIW antenna designs

Ref.	Resonant frequencies (GHz)	Minimum isolation (dB)	Gain (dBi)	Cross polarization (dB)	FTBR (dB)	Size (λ_g^2)	No. of ports
[3]	1.05/1.45/2.0/2.52/3.45/4.17/5.25/5.8/28	~10	0.9/1.35/1.72/2.43/3.2/4.35/4.47/4.49/10.2	N.R.	N.R.	0.068	1
[15]	5.2/5.5/5.8/6.2/6.8	>20	5.2/6.8/5.1/4.6/4.2	15	>14.2	0.28	5
[16]	2.29/2.98/3.65/4.37/5.08	>29.31	3.59/4.55/3.91/5.70/4.92	5	N.R.	0.23	5
[17]	5.33/5.76/6.31/6.86/7.34/7.8	>23.42	4.5/4.94/4.9/5.12/6.12/6.6	10	>10	0.39	6
[18]	2.29/2.96/4.3/5.0/5.61/6.18	>27.01	3.73/4.35/5.57/5.46/4.73	5	>17	0.173	6
[19]	4/5.8/6.6/7.8/9.8/10.68	>27	4.9/5.11/5.4/5.43/5.32/5.3	17	N.R.	0.14	6
[20]	5/5.17/5.32/5.53/5.62/5.72	>29	5.32/5.68/5.41/5.91/5.43/5.14	20	N.R.	0.457	6
[21]	5.15/5.67/6.18/6.6/7.18/7.85/8.25/8.85	>20	3.9/3.2/4.05/4.14/3.8/3.37/3.55/3.28	15	N.R.	0.544	8
[22]	3.54/3.81/4.12/4.5/4.85/5.22/5.5/5.87	>30	4.07/4.3/4.72/5.11/4.43/4.51/4.97/4.47	10.5	>20	0.55	8
[23]	3.35/3.58/3.73/3.91/4.09/4.32/4.61/4.96	>23	4.53/4.62/4.67/4.74/3.83/3.89/3.42/3.55	11	N.R.	0.44	8
This work	2.7/3/3.3/3.6/3.9/4.2/4.5/4.72	>34	4.4/4.19/4.11/4.03/4.19/4.28/5.2/5.44	24.2	>10.4	0.58	8

Note: N.R.: not reported.

are depicted in Figure 13(b). The measured efficiency and gain are better than 70% and 4.03 dBi, respectively. A slight deviation in measured efficiency occurs due to an increase in directivity caused by a decrease in half-power beamwidth, as seen in Figure 15. As the octagon is divided into equal triangles, the radiating elements at higher frequencies have relatively larger apertures than those radiating at lower operating frequencies. This leads to an increase in the gain of each antenna port as the resonant frequency increases. The measured efficiency is better than 70%. Figure 14(a)–14(f) presents the measured and simulated isolation values. The measured isolation is better than 34 dB among all the ports. Figure 15 depicts the radiation patterns for each port at their respective operating frequency. The antenna has a measured cross-polarization level below −24.2 dB in the boresight direction in all bands. The FTBR is more than 10.4 dB in all bands. The measured antenna parameters for each port at the respective frequency are listed in Table 2. A comparison of various performance parameters of the proposed work with previous work is summarized in Table 3. This antenna provides a low co-to-cross polarization level and high isolation among [3, 15–23] with similar values of gain.

Conclusion

This paper proposes a self-octuplexing SIW cavity-backed slot antenna for octa-band wireless communication services. All bands can be independently tuned to operate at the desired frequency according to the required functionality. The antenna achieves a low co-to-cross polarization level and high isolation with moderate gains. This work offers designers flexibility in accommodating multiple functionalities in a single device compared to previous SMA designs. This antenna is useful for 5 G communication, wireless local area network, standard C-band, super-extended C-band, LMI-C-band, radio navigation services, amateur radio, satellite communication, and other multifunction applications.

Acknowledgements. We would like to thank the Science and Engineering Research Board (SERB), DST, Govt. of India, for providing basic infrastructure for this work under the sanctioned project number SRG/2022/000664. We would also like to thank Dr. B. R. Ambedkar NIT Jalandhar, for providing fabrication facility under the sanctioned project number NITJ/DRC/4710.

Competing interests. The authors report no competing interests.

1. **Alhaj NA, Jamlos MF, Manap SA, Abdelsalam S, Bakhit AA, Mamat R, Jamlos MA, Gismalla MSM and Hamdan M** (2023) Integration of hybrid networks, AI, ultra massive-MIMO, THz frequency, and FBMC modulation towards 6G requirements: a review. *IEEE Access* **12**, 483–513. https://doi.org/10.1109/ACCESS.2023.3345453

2. **Rahmani H, Shetty D, Wagih M, Ghasempour Y, Palazzi V and Carvalho NB** (2023) Next-generation IoT devices: sustainable eco-friendly manufacturing, energy harvesting, and wireless connectivity. *IEEE Journal of Microwaves* **3**, 237–255. https://doi.org/10.1109/JMW.2022.3228683
3. **Hussain R** (2021) Shared-aperture slot-based sub-6-GHz and mm-Wave IoT antenna for 5G applications. *IEEE Internet of Things Journal* **8**, 10807–10814. https://doi.org/10.1109/JIOT.2021.3050383
4. **Niu B and Tan J** (2019) Hexa-band SIW cavity antenna system integrating two antennas with high isolation. *Electronics Letters* **55**, 505–506. https://doi.org/10.1049/el.2019.0266
5. **Sun X, Zeng G, Yang H-C and Li Y** (2012) A compact quadband CPW-fed slot antenna for M-WiMAX/WLAN applications. *IEEE Antennas and Wireless Propagation Letters* **11**, 395–398. https://doi.org/10.1109/LAWP.2012.2192901
6. **Erkelenz K, Bohl LP, Sieganschin A and Jacob AF** (2021) A compact K-/Ka-band rectangular-to-coplanar waveguide transition with integrated diplexer. *IEEE Microwave and Wireless Components Letters* **31**, 642–645. https://doi.org/10.1109/LMWC.2021.3064673
7. **Liu H, Xu W, Zhang Z and Guan X** (2013) Compact diplexer using slotline stepped impedance resonator. *IEEE Microwave and Wireless Components Letters* **23**, 75–77. https://doi.org/10.1109/LMWC.2013.2238912
8. **Iqbal A, Al-Hasan M, Mabrouk IB and Nedil M** (2021) Ultracompact quarter-mode substrate integrated waveguide self-diplexing antenna. *IEEE Antennas and Wireless Propagation Letters* **20**, 1269–1273. https://doi.org/10.1109/LAWP.2021.3077451
9. **Priya S, Kumar K, Dwari S and Mandal MK** (2020) Circularly polarized self-diplexing SIW cavity-backed slot antenna. *IEEE Transactions on Antennas and Propagation* **68**, 2387–2392. https://doi.org/10.1109/TAP.2019.2938576
10. **Priya S and Dwari S** (2020) A compact self-triplexing antenna using HMSIW cavity. *IEEE Antennas and Wireless Propagation Letters* **19**, 861–865. https://doi.org/10.1109/LAWP.2020.2982533
11. **Kumar K and Dwari S** (2017) Substrate integrated waveguide cavity-backed self-triplexing slot antenna. *IEEE Antennas and Wireless Propagation Letters* **16**, 3249–3252. https://doi.org/10.1109/LAWP.2017.2771510
12. **Priya S, Dwari S, Kumar K and Mandal MK** (2019) Compact self-quadruplexing SIW cavity-backed slot antenna. *IEEE Transactions on Antennas and Propagation* **67**, 6656–6660. https://doi.org/10.1109/TAP.2019.2925124
13. **Kumar SP, Dwari S and Mandal MK** (2020) 'Self-quadruplexing circularly polarized SIW cavity-backed slot antennas. *IEEE Transactions on Antennas and Propagation* **68**, 6419–6423. https://doi.org/10.1109/TAP.2020.2970101
14. **Shekhar S, Priya S and Kumar K** (2024) A compact self-quintuplexing antenna by HM-SIW cavity. *International Journal of Microwave and Wireless Technologies* **16**, 1561–1569. https://doi.org/10.1017/S1759078724001259
15. **Chaturvedi D, Kumar A, Althuwayb AA and Ahmadfard F** (2023) SIW-backed multiplexing slot antenna for multiple wireless system integration. *Electronics Letters* **59**, e12826. https://doi.org/10.1049/ell2.12826
16. **Barik RK and Koziel S** (2023) Design of compact self-quintuplexing antenna with high-isolation for penta-band applications. *IEEE Access* **11**, 30899–30907. https://doi.org/10.1109/ACCESS.2023.3262295
17. **Dash SKK, Cheng QS, Barik RK, Jiang F, Pradhan NC and Subramanian KS** (2021) A compact SIW cavity-backed self-multiplexing antenna for hexa-band operation. *IEEE Transactions on Antennas and Propagation* **70**, 2283–2288. https://doi.org/10.1109/TAP.2021.3112626
18. **Barik RK and Koziel S** (2022) A compact self-hexaplexing antenna implemented on substrate-integrated rectangular cavity for hexa-band applications. *IEEE Transactions on Circuits and Systems II: Express Briefs* **70**, 506–510.
19. **Melouki N, PourMohammadi P, Nasseri H, Ahmed F, Iqbal A and Hocini A** (2023) Ultra-compact Quarter-Mode SIW self-hexaplexing antenna for C-band and X-band applications. *IEEE Antennas and Wireless Propagation Letters* **23**, 995–999. https://doi.org/10.1109/LAWP.2023.3340878
20. **Jayaprakash V, Chandu D, Barik RK and Koziel S** (2024) Compact substrate-integrated hexagonal cavity-backed self-hexaplexing antenna for sub-6 GHz applications. *IEEE Access* **12**, 54397–54404. https://doi.org/10.1109/ACCESS.2024.3388606
21. **Pradhan NC, Koziel S and Subramanian KS** (2024) Substrate integrated waveguide-based frequency-tunable self-octaplexing antenna. *AEU-International Journal of Electronics and Communications* **176**, 155129.
22. **Rani A and Das S** (2024) A high isolation SIW self-octaplexing antenna with independent frequency tuning capability. *IEEE Antennas and Wireless Propagation Letters* **23**, 1954–1958. https://doi.org/10.1109/LAWP.2024.3375599
23. **Srivastava G, Mohan A, Kanaujia BK and Matekovits L** (2024) Compact self-octaplexing circular EMSIW antenna for sub-6 GHz communication systems. *IEEE Access* **12**, 154173–154181. https://doi.org/10.1109/ACCESS.2024.3479419
24. **Pozar DM**. (1998) *Microwave Engineering*. New York, NY, USA: Wiley.
25. **Xu F and Wu K** (2005) Guided-wave and leakage characteristics of substrate integrated waveguide. *IEEE Transactions on Microwave Theory & Techniques* **53**, 66–73. https://doi.org/10.1109/TMTT.2004.839303
26. **Marcuvitz N**. (1951) *Waveguide Handbook*. Edison, NJ, USA: IET.



Swapnil Shekhar received his B.E. degree in Electronics and Communication Engineering from Thapar Institute of Engineering and Technology, Patiala, India, in 2019 and received his M.Tech. degree from Sant Longowal Institute of Engineering and Technology, Sangrur, India, in 2023. He is currently pursuing his Ph.D. degree from the Department of Electrical Engineering, Indian Institute of Technology, Delhi, India. His research interests include the development of novel antennas, SIW, smart sensors, and their integration.



Kundan Kumar received his B.Tech. in Electronics and Communication Engineering in 2012, M.Tech. and Ph.D. in Electronics and Communication Engineering from the Indian Institute of Technology (ISM), Dhanbad, Jharkhand, India, in the year 2015 and 2020, respectively. Dr. Kumar is working as an Assistant Professor in the Department of Electronics and Communication Engineering at Dr. B R Ambedkar National Institute of Technology Jalandhar, Punjab, India. Prior to this, he worked as an Assistant Professor in the Department of Electronics and Communication Engineering at PEC Chandigarh and SLIET Longowal, respectively. Dr. Kumar was continuously qualified seven times for the Graduate Aptitude Test in Engineering in the subject of Electronics and Communication Engineering and was in the top 0.76% of students in 2013. He was also continuously qualified twice for the National Eligibility Test for Assistant Professor in Electronic Science under the University Grants Commission in June 2014 and December 2014. Dr. Kumar received the Research Publication Award by IIT Dhanbad in the year of 2017 and the Research Project Award by SLIET Longowal in the year of 2023. Dr. Kumar has published 25 research papers in refereed International Journals (like *IEEE Transactions on Antennas and Propagation, IEEE Antennas and Wireless Propagation Letters*, etc.) and Conferences. Dr. Kumar delivered expert talks in several institutes. He is a regular reviewer of various refereed International Journals like IEEE *Transactions on Antennas and Propagation, IEEE Antennas and Wireless Propagation Letters*, etc. His research interests include 5G antennas and circuits, RF and millimeter wave antennas, intelligent antennas for cognitive radio, characterization of dielectric material, modeling and analysis of SIW-based antennas, SMAs, RF planar circuits, RF/microwave sensors, and computational EMs.

https://doi.org/10.1017/S175907872610302X Published online by Cambridge University Press



Shruti Priya received her B.Tech. in Electronics and Communication Engineering in 2012 from Dr. M. G. R. Educational and Research Institute, Chennai, India, M.Tech. in Digital Communication in 2015 from RGPV, Bhopal, India and PhD from Indian Institute of Technology (ISM) Dhanbad, India. She worked as a post-doctoral fellow and Research Associate at the Institute for Plasma Research, Gandhinagar, India, and the Indian Institute of Technology Mandi, India, respectively. Shruti Priya has published several research papers in refereed International Journals and Conferences. Her research interests are in SIW-based antennas, multiband antennas, and SMAs.



Nitesh Kashyap is an Assistant Professor in the Department of Electronics and Communication Engineering at Dr. B.R. Ambedkar National Institute of Technology, Jalandhar. He holds a B.Tech. and M.Tech. in Electronics and Communication Engineering, and earned his Ph.D. with a specialization in planar antennas. With over 10 years of experience in teaching and research, he has published more than 31 research papers in reputed journals and conferences, along with several book chapters. He has supervised one Ph.D. scholar and is currently guiding four more. Additionally, he has mentored 11 M.Tech. dissertations across various domains of communication and microwave engineering.



Surinder Singh was born in Hoshiarpur, Punjab, India, in 1975. He received the B.Tech. degree from Dr. B. R. Ambedkar REC, Jalandhar, India, in 1997, and the M.Tech. degree from the Guru Nanak Dev Engineering College, Ludhiana, India, in 2003, and the Ph.D. degree from Thapar University, Patiala, India, in 2007. Currently, he has been a Professor at Sant Longowal Institute of Engineering and Technology, Longowal, Sangrur, Punjab, since 2013. He has around 230 research papers, out of which 126 are in SCI international journals with Thomson Reuters Impact Factor and 104 are in international and national conferences. He is also handling various research projects and is a reviewer of many international journals and conferences. His field of interest includes optical fiber communication and networks, antennas, and optical sensor design.

https://doi.org/10.1017/S175907872610302X Published online by Cambridge University Press